IEEE Access
Multidisciplinary | Rapid Review | Open Access Journal

Received February 28, 2021, accepted March 22, 2021, date of publication April 5, 2021, date of current version April 26, 2021.

Digital Object Identifier 10.1109/ACCESS.2021.3071130

FPGA-Based High-Performance Double-Loop PDF Control Strategy for PMSM

HAITAO DONG, MINGCHEN XIAO, ZHAOJUN LI, SHUAITAO ZHANG, AND JIANGUO CHEN
School of Mechanical Engineering, Guangxi University, Nanning 530004, China

Corresponding author: Haitao Dong (surge_d@163.com)

This work was supported by the Cernet Next Generation Internet Technology Innovation Project under Grant NGII20190312.

ABSTRACT Due to the large overshoot and poor disturbance rejection impact the control accuracy of the permanent magnet synchronous motor (PMSM) in the proportional–integral–derivative (PID) control mode. In this paper, we propose an optimal double-loop pseudo-derivative feedback (PDF) control strategy. Firstly, to obtain high-precision feedback current and minimize the influence of sampling delay, a double-feedback PDF control structure is configured based on the Σ–Δ sampling modulation and Sinc3 filter. Secondly, we adopt an instant-sampling and instant-update (ISIU) strategy based on a field-programmable gate array (FPGA), which can reduce the update delay of the pulse-width modulation (PWM), and design the hardware timing diagram, accordingly. Then, based on the influence of the closed-loop pole position on the dynamic performance of the system and the saturation characteristics of the power device, the PDF parameters tuning method of the current loop and speed loop is proposed. Finally, the system performance under different control strategies is compared and analyzed through simulations and experiments. The results show that the optimal double-loop PDF control strategy proposed in this paper can considerably expand the bandwidth of the current loop and has better disturbance rejection.

INDEX TERMS Permanent magnet synchronous motor (PMSM), PDF control strategy, Σ–Δ sampling update strategy, double-feedback structure.

I. INTRODUCTION

Permanent magnet synchronous motors (PMSMs) are widely used in the field of motion control because of their high efficiency, high-power density, and high precision [1], [2]. In the three-loop cascade control method, the response performance of the innermost current loop directly affects the control performance of the two outer loops. Thus, the current loop should have high response bandwidth and high steady-state accuracy. The speed loop as the middle loop requires minimum speed response overshoot and strong anti-load torque fluctuation ability. The outermost position loop requires the position response with no overshoot and high positioning accuracy. The traditional servo control strategy is sufficient for industrial control scenarios with low precision and poor performance. However, in special industrial control scenarios required high control accuracy, such as tension control and constant torque control, an AC servo system should be with no overshoot, high precision and fast torque response, and strong disturbance rejection [3]. Realization of the goal requires high-precision current sampling and the design of high-performance double-loop control strategy.

A commercial Hall current sensor or shunt resistor is often used in sampling phase current. Although this method is simple and inexpensive, but it is low sampling accuracy, and not suitable for scenarios requiring high-precision current control [4]. The Σ–Δ modulation sampling chip applies oversampling technology to meet the requirements for high-precision current sampling by adjusting flexibly with the filter coefficient [5], [6].

The commercial servo drivers simplify the system to a DC motor model by decoupling method, and apply PI control in current loops [7], [8]. The basic principle is to linearly adjust the current error of d–q axis by the proportional-integral control and combine the feedforward method to eliminate the influence of d–q axis coupling relationship on the control performance of PMSM. The PI control parameters of current loop are usually adjusted by classical I–type system. the controller is simple structure, mature technology and good stability, but it will lead to large overshoot while pursuing high-speed response, and affect the control accuracy. Thus, it is not suitable for high-performance control scenarios [9].

The associate editor coordinating the review of this manuscript and approving it for publication was Nasim Ullah.

Furthermore, the predictive current control algorithm has been applied to commercial servo drivers, and offers a fast response with no overshoot. Based on the model prediction theory, the algorithm calculates the current value at the next moment by using the discrete voltage equation and the mathematical model of voltage source inverter, and obtains the voltage control value by combining with the current given value [10], [11]. Compared with PI control, the advantage of predictive control is that it reduces the delay of the current loop and improves the bandwidth of the current loop. However, because the algorithm is more sensitive to the fluctuation of parameters, it needs an observer to improve the robustness [12], [13], which is complex to implement and more sensitive to current harmonic disturbances.

As the middle loop of the entire servo system, the speed loop ensures that the motor runs smoothly at the speed command. In the scenarios with high requirements for constant speed control, the speed response should have strong resistance to load torque disturbance to ensure that the system can quickly track the speed command without overshoot. The speed loop enhances system rigidity to minimize fluctuations in speed and quickly return to the steady-state speed when the load torque changes, and it is critical in improving the overall performance of an AC servo system [14], [15]. When using PI control, the response of the speed loop exhibits large overshoot, and the system is more sensitive to load disturbance. Scholars have introduced fuzzy tuning and adaptive control to reduce the overshoot in PI controllers [16], [17], but these measures have not significantly improved the disturbance rejection of the system.

Without introducing the differential component, the PDF controller differentially process the feedback signal and the forward path signal by changing the PI controller structure. On the basis of retaining the PI control advantages, it can suppress the system overshoot and improve the disturbance rejection [18]. Bo *et al.* improved the disturbance rejection of the system by assigning the closed-loop pole position [19]. Their tuning method is simple and intuitive, but the response speed of PDF controller tuned by this method is slower than that of the general PI controller. This is not suitable for the fast torque control. By introducing a IIR low-pass filter into the control loop and combining with fuzzy inference, Cheng and Li designed a fuzzy PDFF-IIR controller [20]. To a certain extent, it improved the speed loop responsiveness and disturbance rejection, but the algorithm was complex and difficult to implement in engineering. Using the advantages of field-programmable gate array (FPGA) high-speed operation, Karthikeyan *et al.* proposed a PDF control method that could combine with direct torque control to effectively improve response speed [21], [22]. However, the direct torque control introduced more current harmonics, system performance was not improved overall. In order to improve the disturbance rejection of the system, Xing *et al.* combined the reduced-order load torque observer with the PDF controller used Phelan tuning method, but this design ignored some influence factors such as PWM update delay [23]. To achieve sensorless control of PMSM, Karthikeyan *et al.* developed PDF controller by using MARS estimator [24], and Li *et al.* designed PDF controller to improve the robustness of the system [25]. However, none of them gave a clear method to tune PDF parameters.

This research aims to design optimal double-loop PDF control strategy based on the FPGA to expand the bandwidth of current loop. The contributions of this paper are as follows.

1) Based on FPGA, combined with the instant-sampling and instant-update (ISIU) strategy, we designed the asynchronous Sinc3 demodulation filter structure and the corresponding hardware timing diagram. This method makes full use of FPGA on-chip logic resources and minimizes the loop delay on the basis of ensuring high-precision current sampling.
2) We construct a double-loop PDF control mathematical model, and prove that the third-order system achieves the best dynamic performance when the characteristic roots coincide.
3) We analyze the relationship between the system response performance and the pole position distribution in theory, and propose a double-loop PDF parameter tuning method for PMSMs. This method can effectively improve the dynamic response of the system.

The remainder of this paper is organized as follows. Preliminaries are introduced in Section II. Section III presents the double-loop PDF control strategy of PMSM, including optimal designs of PDF current controller and PDF speed controller. Section IV gives FPGA implementation of double-loop PDF controller. Section V demonstrates the effectiveness of the proposed approach by simulations and experiments. Finally, the conclusion is given in Section VI.

II. PRELIMINARIES

A. Σ − Δ SAMPLING AND SINC3 FILTERING PRINCIPLE

The sampling module consists of a second-order Σ−Δ modulation and a Sinc3 filter. The Σ−Δ modulation samples motor phase current and converts the analog electrical signal into a 1–bit high-speed digital stream of 20 Mbps. The Sinc3 filter demodulates the digital code stream that is generated through the Σ−Δ modulation. The overall structure of the sample-demodulation system is shown in Fig. 1. By setting an appropriate decimation rate, the current sampling module can filter out most of the system noise and restore the sampled current signal without loss.

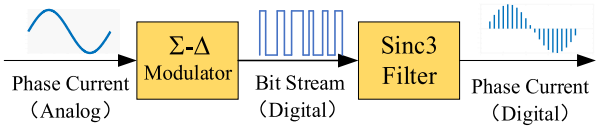

FIGURE 1. Σ−Δ modulation structure.

Through Σ−Δ modulation, the sampling delay generated by the analog signal can be ignored, the quantization noise is pushed to the high-frequency band, and its gain in the signal bandwidth is greatly attenuated to achieve noise shaping.

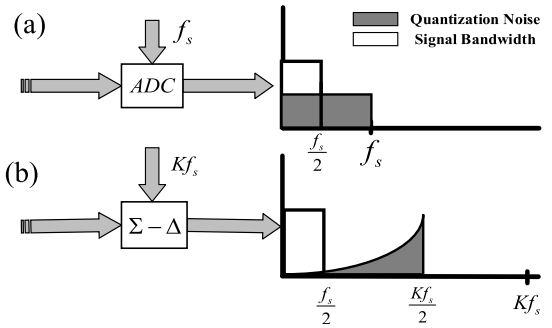

FIGURE 2. Noise comparison of sampling methods (a: A/D sampling, b: Σ−Δ modulation).

The quantization noise distribution of A/D sampling and Σ−Δ modulation sampling is shown in Fig. 2.

A Sinc3 filter consumes few logic resources and is easy to implement in hardware. The transfer function of an N–order Sinc filter is given as (1).

$$H(z) = \left(\frac{1}{DR}\sum_{\mu=0}^{DR-1} z^{-\mu}\right)^N = \left(\frac{1}{DR}\frac{1-z^{-DR}}{1-z^{-1}}\right)^N \quad (1)$$

where DR is the decimation rate. The order of Sinc filter is usually 1–bit higher than that of the Σ−Δ modulation. Herein, the second-order Σ−Δ modulation chip is selected, and the third-order Sinc3 filter is used to demodulate and filter the current.

B. PWM UPDATE STRATEGY

In an AC servo system, the control chip generates a triangular carrier signal by counting the timer continuously. The chip then compares the carrier signal with the modulation wave obtained using the vector algorithm to generate the left-right symmetrical PWM waveform. The time taken to generate a triangular carrier is considered as the PWM cycle, and the moment when the timer starts counting is regarded as the start of PWM cycle. The duty cycle output is updated for each PWM cycle. The current loop can adopt the moment or overflow point as the sampling mark to trigger current sampling and vector calculation. DSP and ARM chips are restricted by the limitations of computing power and serial execution of the software. Hence, the single-sampling and single-update (SSSU) is usually adopted for the update mode of the duty cycle. The typical SSSU method is shown in Fig. 3. The current sampling value is triggered at the k^{th} time point, and the duty cycle of PWM is updated at the $(k+1)^{\text{th}}$ moment. The chip can complete the current sampling and vector calculation in a PWM cycle. Let T_{pwm} be the PWM update period, the loop delay $t_\sum$ introduced by the system update can be shown in (2).

$$\begin{cases} t_d = T_{pwm} \\ t_{pwm} = 0.5 \cdot T_{pwm} \\ t_\sum = t_d + t_{pwm} = 1.5T_{pwm} \end{cases} \quad (2)$$

An FPGA can substantially shorten the calculation time of vector control owing to its powerful computing power

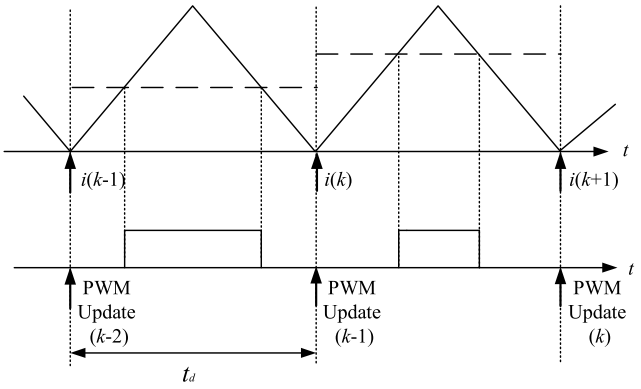

FIGURE 3. SSSU method.

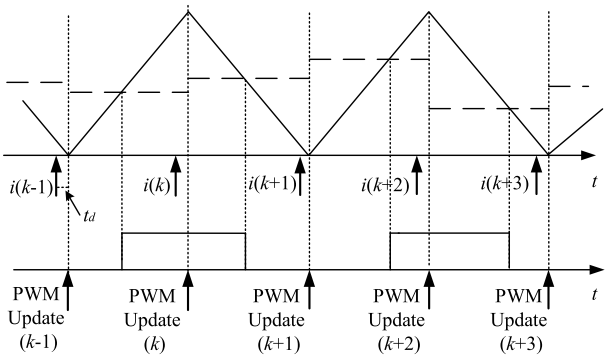

FIGURE 4. ISIU method.

and parallel execution characteristics [26]. In a PWM cycle, the current loop can complete the synchronous calculation and update of two duty cycle, where the updates occur at the start of the timer and underflow time, respectively. The ISIU strategy is shown in Fig. 4, and the loop delay introduced by the system update is given by (3).

$$\begin{cases} t_d \approx 0 \\ t_{pwm} = 0.25 \cdot T_{pwm} \\ t_\sum = t_d + t_{pwm} = 0.25 \cdot T_{pwm} \end{cases} \quad (3)$$

In contrast with the SSSU strategy, the ISIU strategy can reduce the PWM update delay to 0.25 T_{pwm}.

C. MATHEMATICAL MODEL OF PMSM

The voltage equation of a surface-mounted permanent magnet synchronous motor (SPMSM) under field-oriented control (FOC) can be described as (4).

$$\begin{cases} \begin{bmatrix} u_d \\ u_q \end{bmatrix} = \begin{bmatrix} R & -L\omega_e \\ L\omega_e & R \end{bmatrix} \begin{bmatrix} i_d \\ i_q \end{bmatrix} + \begin{bmatrix} L & 0 \\ 0 & L \end{bmatrix} \\ \qquad \begin{bmatrix} \frac{d}{dt} i_d \\ \frac{d}{dt} i_q \end{bmatrix} + \begin{bmatrix} 0 \\ \omega_e \psi \end{bmatrix} \\ T_e = \frac{3}{2}\frac{P}{2}\psi i_q \end{cases} \quad (4)$$

where u_d and u_q are the $d-$axis and $q-$axis voltages, i_d and i_q are the $d-$axis and $q-$axis currents, R is the armature

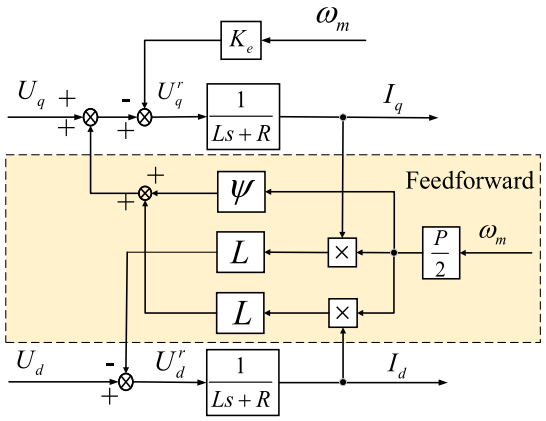

FIGURE 5. Voltage feedforward control for decoupling.

resistance, L is the equivalent inductance of d–q axis, ω_e is the mechanical angular velocity, Ψ is the permanent magnet flux linkages, T_e is the electromagnetic torque, and P is the number of poles. During the rotation of the motor, there is a cross-coupling relationship between the d–q axis, and the current loop is decoupled by introducing voltage feedforward. The decoupled current loop structure is drawn in Fig. 5, and the expression is shown in (5).

$$\begin{cases} U_q^r(s) = U_q(s) - \omega_e(LI_d(s) + \psi) \\ U_d^r(s) = U_d(s) + \omega_e LI_q(s) \\ \dfrac{I_q(s)}{U_q^r(s)} = \dfrac{1}{Ls+R} \\ \omega_e = \dfrac{1}{2}P\omega_m \end{cases} \tag{5}$$

where K_e is the back electromotive force coefficient, U_d^T and U_q^T are the control voltages of the $d-$axis and $q-$axis after decoupling, and ω_m is the mechanical angular velocity of the rotor.

III. DOUBLE-LOOP PDF CONTROL STRATEGY OF PMSM

A. OPTIMAL DESIGN OF PDF CURRENT CONTROLLER

1) DOUBLE-FEEDBACK STRUCTURE PDF OF CURRENT LOOP

The integral component accumulates the system error signal, which requires high precision of the feedback signal, but is not sensitive to the response delay. Meanwhile, the proportional and differential components adjust the system error in time, and they are more sensitive to the system delay but not to the precision of feedback signal [27]. Analyzing the PDF structure and the characteristics of Sinc3 filtering and demodulation, it can be seen that a large sampling delay is introduced while obtaining high-precision sampling current. The relationship between sampling precision and delay can be flexibly adjusted by setting the filter decimation rate. Under 20MHZ sampling frequency, when Sinc3 filter adopts the typical decimation rate, its corresponding sampling precision and delay are shown in Table 1.

Combining the PDF control strategy with the decimation characteristics of Sinc3 filter, the closed-loop system of current loop is constructed using double-feedback structure,

TABLE 1. Data accuracy and delay.

Decimation rate	Data precision (bit)	Transmission delay (us)
32	14	2.35
64	17	4.75
128	20	9.55
256	23	19.15

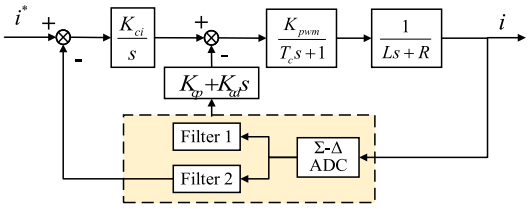

FIGURE 6. Block diagram of double-feedback structure PDF of the current loop.

as shown in Fig. 6. This structure can obtain high-precision current feedback and minimize the impact of sampling delay on control performance.

2) THE PDF OPTIMIZATION CONTROL STRATEGY FOR CURRENT LOOP

Since the double-feedback structure of Σ–Δ demodulation is adopted to sample the current, the sampling delay is so small that its influence can be ignored. In addition, to simplify the analysis process, the $q-$axis is presented for the loop analysis. The PDF control block diagram of the current loop is shown in Fig. 7. Where K_{cp}, K_{ci}, and K_{cd} are the PDF control parameters, K_{pwm} is the inverter gain constant, and T_c is the loop delay. The closed-loop transfer function of the current loop is shown in (6).

$$\begin{aligned} &G_{current}(s) \\ &= \frac{K_{ci} \cdot c_3}{s^3 + (c_1 + K_{cd} \cdot c_3) \cdot s^2 + (c_2 + K_{cp} \cdot c_3) \cdot s + K_{ci} \cdot c_3} \\ &c_1 = \frac{T_c R + L}{T_c L}, c_2 = \frac{R}{T_c L}, c_3 = \frac{K_{pwm}}{T_c L} \end{aligned} \tag{6}$$

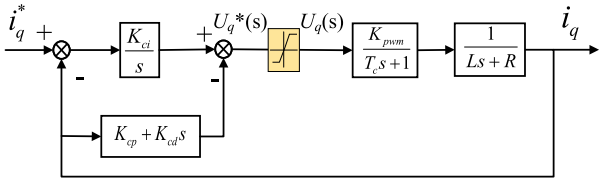

FIGURE 7. Block diagram of the current loop.

When the closed-loop gain is −3dB, the corresponding angular frequency of the above system is ω_{cb} [28]. The relationship between the bandwidth of current loop and system parameters is shown in (7).

$$\begin{aligned} &(K_{ci} \cdot c_3)^2 \\ &= \left[\omega_{cb}^2 + (c_1 + K_{cd} \cdot c_3)^2 - 2 \cdot (c_2 + K_{cp} \cdot c_3)\right] \omega_{cb}^4 \end{aligned} \tag{7}$$

In high-performance current loop control, the actual current should accurately and quickly track the current command

and should be without overshoot. According to the eigenvalue structure theory, when the closed-loop poles are on the negative real axis, the system can track the current command without overshoot. Let the poles of the closed-loop transfer function be $-m_1$, $-m_2$ and $-m_3$. Then, the system poles relationship can be obtained, as shown in (8).

$$(s+m_1)(s+m_2)(s+m_3) = s^3 + (c_1 + K_{cd} \cdot c_3) \cdot s^2 + (c_2 + K_{cp} \cdot c_3) \cdot s + K_{ci} \cdot c_3 \quad (8)$$

Equation (8) can be simplified to obtain the following relationship between the system characteristic roots and system parameters, as shown in (9).

$$\begin{cases} m_1 \cdot m_2 \cdot m_3 = c_3 \cdot K_{ci} \\ m_1 \cdot m_2 + m_2 \cdot m_3 + m_1 \cdot m_3 = c_2 + c_3 \cdot K_{cp} \\ m_1 + m_2 + m_3 = c_1 + c_3 \cdot K_{cd} \end{cases} \quad (9)$$

Substituting Equation (9) into the closed-loop bandwidth Equation (7) can obtain (10).

$$\left[\omega_{cb}^2 + \underbrace{m_1^2 + m_2^2 + m_3^2}_{①}\right] \omega_{cb}^4 = \underbrace{m_1^2 \cdot m_2^2 \cdot m_3^2}_{②} \quad (10)$$

To maximize the system bandwidth, the value of ① should be minimized, and the value of ② should be maximized. According to the following inequality (11), when the real roots coincide and the above conditions are simultaneously fulfilled, the system bandwidth reaches its maximum.

$$\sqrt[3]{m_1^2 \cdot m_2^2 \cdot m_3^2} \le \frac{m_1^2 + m_2^2 + m_3^2}{3} \quad (11)$$

Let h be the position of the triple real roots of the system. Under the excitation of a step signal with the amplitude a, the response equation of the third-order multiple real roots system is shown in (12).

$$y(t) = L^{-1}\left[\frac{h^3}{(s+h)^3} \cdot \frac{a}{s}\right] = a\left[1 - \underbrace{\left(\frac{h^2 \cdot t^2}{2} + h \cdot t + 1\right) e^{-h \cdot t}}_{①}\right] \quad (12)$$

Equation (12) shows that the exponential function term of the system response equation is always greater than zero, the current has no overshoot, and the response speed is related to the value of its triple poles. For a high-precision control system, the time when the response curve falls within the 2% error band for the last time is considered the system settling time. For a response curve without overshoot, the settling time can be expressed as in (13).

$$\left|\frac{y(t_s) - a}{a}\right| \times 100\% = 2\% \quad (13)$$

Simultaneously solving Equations (12) and (13) obtains (14).

$$h \cdot t_s = 7.5166 \quad (14)$$

Equation (14) shows that the system response becomes faster as the distance from the virtual axis increases. Because of the delay effect of the current loop, the current settling time should be greater than the system equivalent loop delay T_c. Thus, the triple pole position should fall in the following range (15).

$$0 < h < \frac{7.5166}{T_c} \quad (15)$$

Because the rise time of the current response curve is very short, the rise curve can be linearized. The empirical formula for the system bandwidth can be used to obtain, as shown in (16).

$$\frac{0.35}{0.8nT_c} = x \cdot \frac{1}{T_c} \quad (16)$$

where x is the bandwidth conversion coefficient with a range of 0.15–0.2 and n is the delay beat number of the current loop [28]. Equations (14) and (16) can be combined to deduce the engineering settings for the parameters of the current loop, as shown in (17).

$$\begin{cases} K_{cp} = \dfrac{3h^2 - c_2}{c_3}, K_{ci} = \dfrac{h^3}{c_3} \\ K_{cd} = \dfrac{3h - c_1}{c_3}, h = \dfrac{7.5166}{3T_c} \end{cases} \quad (17)$$

The differential component is sensitive to the noise signal in the feedback loop. Hence, it is usually used in combination with a low-pass filter. In the PDF control strategy, because the differential gain is small and has almost the same effect as the proportional component, the proportional gain coefficient can be increased to approximate the proportional-differential linear combination.

B. OPTIMAL DESIGN OF PDF SPEED CONTROLLER

1) THE PDF CONTROL MODEL OF SPEED LOOP

The dynamic torque equation of PMSM can be described as (18).

$$J\frac{d\omega_m(t)}{dt} = K_t i_q(t) - T_L \quad (18)$$

where J is the moment of inertia of the motor, K_t is the torque constant. When the influence of the load torque T_L is not considered, applying the Laplace transform to Equation (18) obtains (19).

$$\frac{\omega_m(s)}{I_q(s)} = \frac{1}{Js} \cdot K_t \quad (19)$$

In the PDF control strategy, the current loop has a fixed beat delay. The equivalent delay nT_c of the current loop and sampling delay T_{ve} of the speed loop can be combined into the total loop delay T_v. The first-order approximation of the equivalent loop delay is given as (20).

$$G_{veq}(s) = \frac{1}{(nT_c + T_{ve})s + 1} = \frac{1}{T_v s + 1} \quad (20)$$

The PDF control block diagram of the speed loop is shown in Fig. 8. K_{vp}, K_{vi} and K_{vd} are the control parameters. Then,

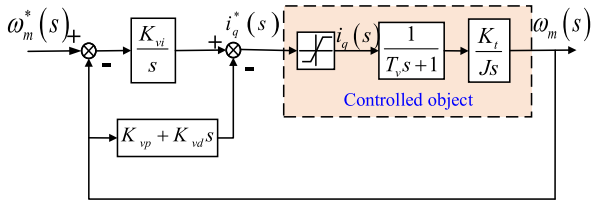

FIGURE 8. Block diagram of the speed loop.

the transfer function of the speed loop with PDF control is shown in (21).

$$G_v(s) = \frac{K_t \cdot K_{vi}}{J \cdot T_v \cdot s^3 + (J + K_t \cdot K_{vd}) \cdot s^2 + K_t \cdot K_{vp} \cdot s + K_t \cdot K_{vi}} \tag{21}$$

2) ANTI-SATURATION PDF OPTIMIZATION CONTROL STRATEGY FOR SPEED LOOP

The speed loop should have roughly the same configurations as those of the current loop. To analyze the influence of the real root position of the speed loop on the system performance, r is adopted to represent the triple real roots position of the speed loop. Fig. 9 shows the simulation results as the triple real roots position of the speed loop gradually moves away from the virtual axis, and Fig. 9(a) shows the three-dimensional diagram of the speed response. According to Equation (14), increasing the r value reduces the system settling time, which facilitates the fast tracking of the current command without overshoot. Due to the current limitations of the power module of the servo system, when the output current of the controller is too large, the controlled object enters the saturation state, and the output current of the controller is reduced to the limited input of the current loop, as shown in Fig. 9(c). At this point, the electrical signal of the input-controlled object is inconsistent with the output signal of the speed loop, and the system is out of balance. The speed response curve rises at a fixed slope, which results in saturation overshoot. To visualize the response characteristics of the system in the saturation state, Fig. 9(b) and (d) show the curves of the system speed and controlled current at the triple real roots $r = 375$ and $r = 1073$, respectively. In the unsaturated state, the system has no overshoot in the speed response and can track the current command within the configured settling time. The controlled current curve is smooth and linear. When the system is in the saturation state, the controlled current curve maintains the maximum amplitude for a period of time, which is directly reflected by the maximum overshoot caused by the speed response. To achieve optimal control of the servo system, the closed-loop pole position of the system should be adjusted according to the saturation limit of the power element.

According to Fig. 8, the transfer function of the controlled object is given as (22).

$$\frac{\omega_m(s)}{I_q(s)} = \frac{K_t}{Js \cdot (T_v s + 1)} \tag{22}$$

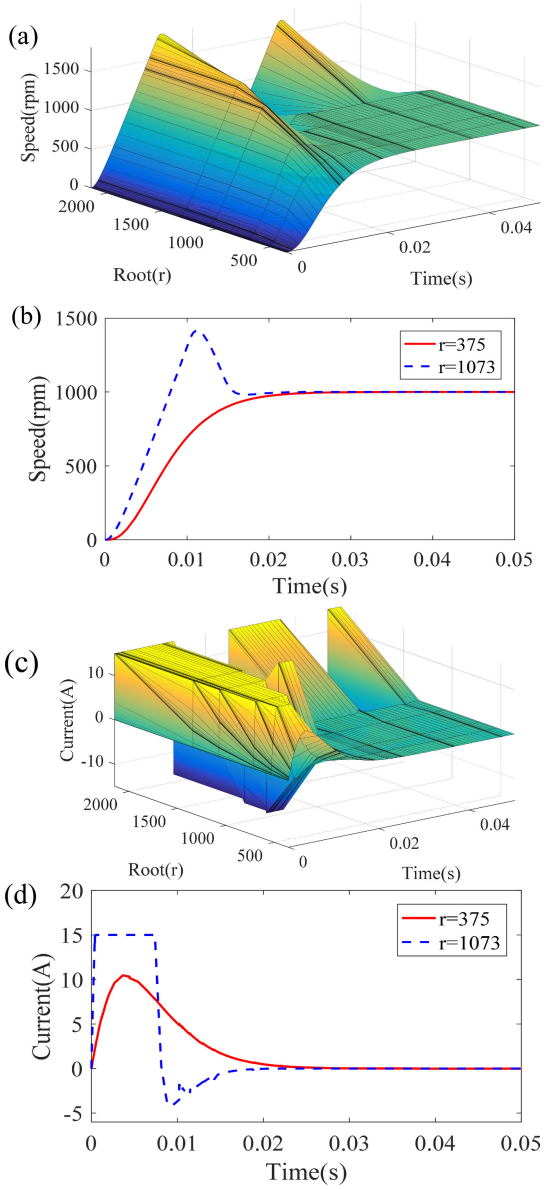

FIGURE 9. Nonlinear system power saturation (a: System speed response, b: System speed response at $r = 375$ and $r = 1073$, c: Current of the controlled object, d: Current of the controlled object at $r = 375$ and $r = 1073$).

Let the output signal of the speed loop be $\omega_m(t)$. Then, $\omega_m'(t)$, $\omega_m''(t)$ are the first and second derivatives, respectively, of the system speed output function. Thus, the energy function $i_q(t)$ of the input-controlled object can be expressed as (23).

$$i_q(t) = \frac{JT_v}{K_t} \cdot \omega_m''(t) + \frac{J}{K_t} \cdot \omega_m'(t) \tag{23}$$

Let A be the step speed command value. Then, the step response of the triple real roots system is shown in (24).

$$\omega_m(t) = A \cdot \left[1 - \left(\frac{r^2 \cdot t^2}{2} + r \cdot t + 1\right) e^{-r \cdot t}\right] \tag{24}$$

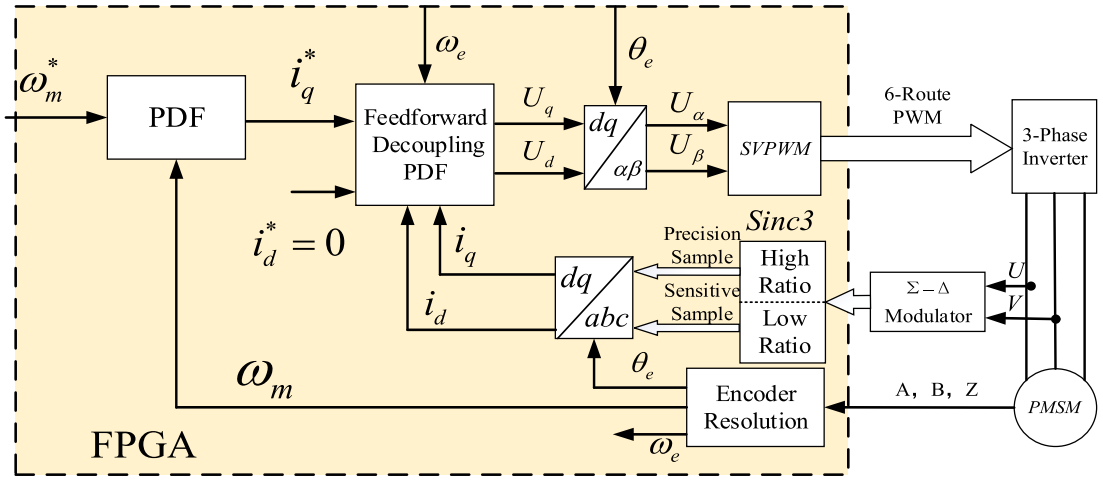

FIGURE 10. Overall structure of digital circuit.

Combining Equation (23) with Equation (24), the current function can be obtained as (25).

$$i_q(g) = A \cdot \frac{JT_v}{K_t} \cdot \left[\left(gr^2 - \frac{1}{2}g^2r^2\right) + \frac{1}{T_v} \cdot \left(\frac{1}{2}g^2r\right)\right] \cdot e^{-g} \tag{25}$$

where $g = r \cdot t$ is a dimensionless number. To keep the system under control, the amplitude of the current output of the controller should be less than the maximum current of system. Fig. 9(d) shows that the unsaturated current signal has two extreme points, and the maximum value is at the first extreme point. The above current function can be derived as (26).

$$g = \frac{(2T_v r - 1) \pm \sqrt{2T_v^2 r^2 - 2T_v r + 1}}{T_v r - 1} \tag{26}$$

To simplify Equation (26), only the higher-order terms are considered. When $g_{\max} \approx 2 - \sqrt{2}$, the input current reaches its maximum value. Let the maximum current allowed to pass through the controlled object be I_{max}. Then, Equation (26) can be used to obtain the triple real roots of the speed loop, as shown in (27).

$$r = \pm\sqrt{\frac{1}{T_v^2} + 101.109 \cdot \frac{K_t I_{\max}}{AJT_v}} - \frac{1}{T_v} \tag{27}$$

When the system is stable, all closed-loop poles lie on the negative real axis (i.e., $-r < 0$). Using the triple real roots tuning method, the PDF control parameters of the speed loop are obtained as (28).

$$\begin{cases} K_{vi} = \dfrac{J \cdot T_v}{K_t} \cdot r^3 \\ K_{vp} = \dfrac{3J \cdot T_v}{K_t} \cdot r^2 \\ K_{vp} = \dfrac{3r \cdot J \cdot T_v - J}{K_t} \\ r = \sqrt{\dfrac{1}{T_v^2} + 101.109 \cdot \dfrac{I_{\max} \cdot K_t}{A \cdot JT_v}} - \dfrac{1}{T_v} \end{cases} \tag{28}$$

Considering the maximum current limitation of the servo system, the energy of the system can be maximized by inversely calculating the triple poles position of the system, which can realize speed control with a high response and no overshoot.

IV. FPGA IMPLEMENTATION OF DOUBLE-LOOP PDF CONTROLLER

A. FPGA CIRCUIT DESIGN

Owing to the ISIU strategy, the current vector control module requires extremely high chip operation speed. In the very short time before the PWM update point, the chip needs to complete tasks such as PDF control strategy, coordinate change, vector calculation and PWM modulation. To ensure the real-time performance of the feedback current calculation, the lead time should be as short as possible, but it is difficult for STM32 and DSP chips to complete the above series of calculations in a short time. FPGA chip has the characteristics of parallel execution, which can considerably reduce the operation delay [29]. The overall structure diagram of the high-performance double-loop PDF of servo system based on FPGA is shown in Fig. 10. The proposed optimal control strategy mainly comprises a filter demodulation module, PDF controller module, coordinate transformation module and SVPWM modulation module. The Sinc3 filter demodulates the sampled bitstream, and the rotor position information is parsed by the encoder module.

The $d-q$ axis current is obtained following the coordinate transformation of the three-phase feedback current, which is fed into the PDF decoupling controller together with the current command for calculation. The expected voltage vector can be obtained. Then, six PWM waves can be outputted through the SVPWM modulation module.

B. FPGA TIMING PLANNING

Because the feedback current values of the Sinc3 filter differ according to the sampling rate with the double-feedback

structure, the proposed PDF control strategy needs to be calculated with two coordinate transformation modules. To maximize the use of on-chip logic resources, the feedback current value with high decimation rate is locked in the integrating path register of the PDF controller after the coordinate transformation. Then, the feedback current is calculated for low decimation rate, and the PDF controller operation is triggered. The proposed method introduces a delay of 12 clock cycles to realize current sampling, but this delay can be ignored for FPGA with high-speed clock.

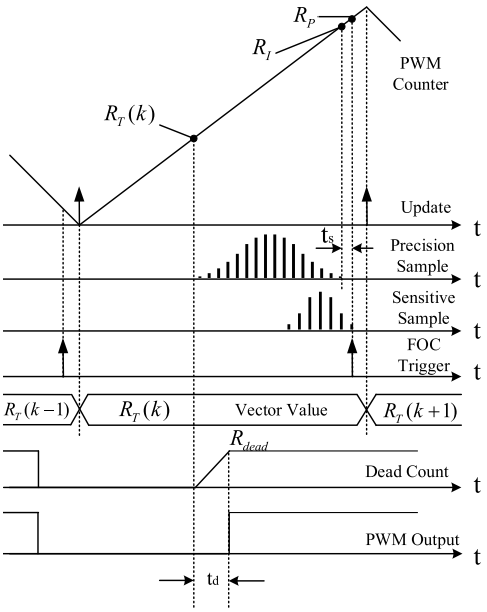

FIGURE 11. FPGA timing planning.

Fig. 11 shows a timing diagram for the proposed PDF control strategy. In addition to the filter demodulation and encoder frequency multiplier modules, other modules are subsequently fired in turn with the PWM counter as the benchmark. In the figure, R_I is the trigger point for calculating the feedback current value with a high decimation rate. R_P is the trigger point for calculating the feedback current value with a low decimation rate and the vector control strategy. $R_T(k)$ is the k^{th} PWM output comparison register value. R_{dead} is the dead time register value. t_s is the time interval for calculating the feedback current, and t_{dead} is the dead time.

V. SIMULATIONS AND EXPERIMENTS

Simulations and experiments are performed using an N0701F PMSM (Park Company) for verifying the proposed control strategy. The parameters of the motor are presented in Table 2. The carrier frequency of the PWM is 16 kHz, and the update frequency of the speed loop is 800 Hz.

A. SIMULATION VERIFICATION

1) CURRENT LOOP

In order to verify the dynamic performance of the proposed algorithm, we conducted a comparative experiment on the

TABLE 2. Motor parameters.

name	unit	Value
Resistance	Ohm	2.27
Inductance	mH	5.23
Rotor inertia	Kg·m^2	1.5E-5
Torque constant	N·m/A	0.120
Viscous Damping	Nm/krpm	1.4 E-3
Poles	P	4
Rated current	A	5.4
Rated power	W	472
Rated torque	N·m	0.52
Rated voltage	V	340
Rated speed	rpm	7500

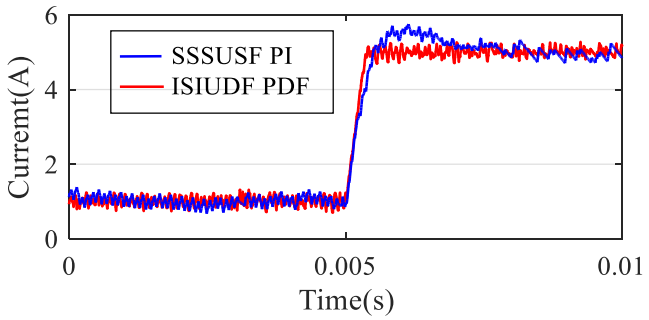

FIGURE 12. Current response.

step response of the SSSU single-feedback PI (SSSUSF PI) and ISIU double-feedback PDF (ISIUDF PDF). In order to keep the simulation consistent with the experiment, an initial current command of 1 A is given to overcome the influence of friction torque when starting the motor. Then, a current step command with an amplitude of 4 A is applied to analyze the current loop response. As shown in Fig. 12, the current response of the ISIUDF PDF control strategy has no overshoot and is faster than that of the SSSUSF PI control strategy, because the current loop sampling delay of proposed control strategy is shortened.

In order to compare the current loop performance of single-feedback structure and double-feedback structure PDF, we conducted a step response experiment of the current loop under the same SSSU PWM update strategy. Sinc3 filters with decimation rate of 128 and 256 are used in the SSSU single-feedback PDF (SSSUSF PDF) structure, and filters with decimation rate of 16 and 256 are used in the SSSU double-feedback PDF (SSSUDF PDF) structure. The time-domain and frequency-domain response curves of the two feedback structures with different filter decimation rate are shown in Fig. 13(a) and (b), respectively. From Fig. 13(a), we note that the filter response to the SSSUSF PDF structure with a decimation rate of 128 oscillates. When the decimation rate is increased to 256, the oscillation trend of SSSUSF PDF structure response will increase, and even cause the system to diverge. The SSSUDF PDF response with 16 and 256 decimation rates can obtain high-precision current sampling while ensuring the system

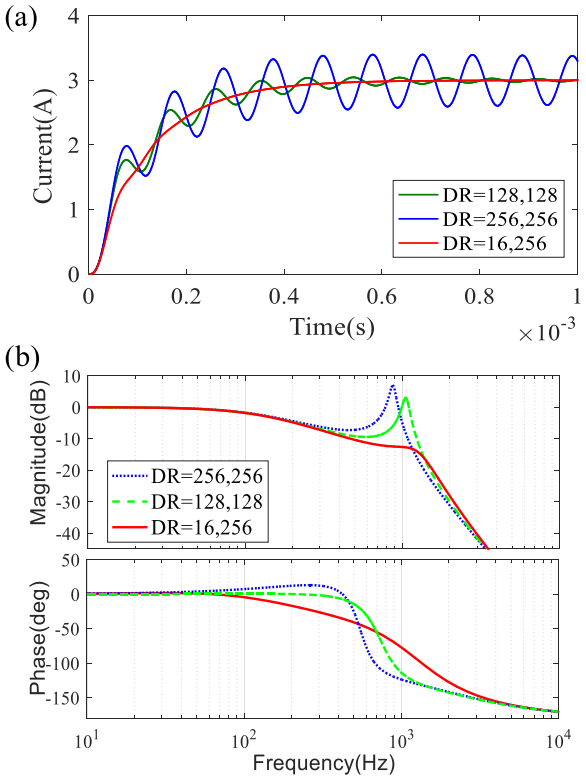

FIGURE 13. Time-frequency response comparison diagram of two PDF structures (a: Time-domain response, b: Frequency-domain response).

has high dynamic performance. From the frequency domain curve in Fig. 13(b), we can see that the single-feedback PDF structure produces obvious convex peak at high decimation rate, and the phase lag is serious near the frequency of 1kHz, while the double-feedback PDF structure does not have the above problems.

Fig. 14 shows the time domain and frequency domain curves of the SSSUSF PDF control strategy, ISIU single-feedback PDF (ISIUSF PDF) control strategy and ISIU double-feedback PDF (ISIUDF PDF) control strategy. Fig. 14(a) shows that the ISIU strategy effectively improves the response speed of the system, but the ISIUSF PDF structure produces oscillates that degrade the control performance of the system. With the ISIUDF PDF structure, the current response is stable, fast, and without overshoot while tracking the current command. Fig. 14(b) shows that the ISIUSF PDF improves the system bandwidth to a certain extent, but it exacerbates the convex peak. The ISIUDF PDF can effectively shorten the loop delay and suppress the convex peak, thus it can further expand the current loop bandwidth. Their closed-loop bandwidth is shown in Table 3.

2) SPEED LOOP

When the ISIUDF PDF control strategy is adopted for the current loop, simulations are performed to analyze the speed response using the triple poles tuning method PDF (TPM PDF) and Richard M. Phelan tuning method PDF [30] (MPM PDF), respectively.

TABLE 3. Closed-loop system bandwidth.

Control Strategy	SSSUSF PDF	ISIUSF PDF	ISIUDF PDF
System bandwidth	613 Hz	1522 Hz	1998 Hz

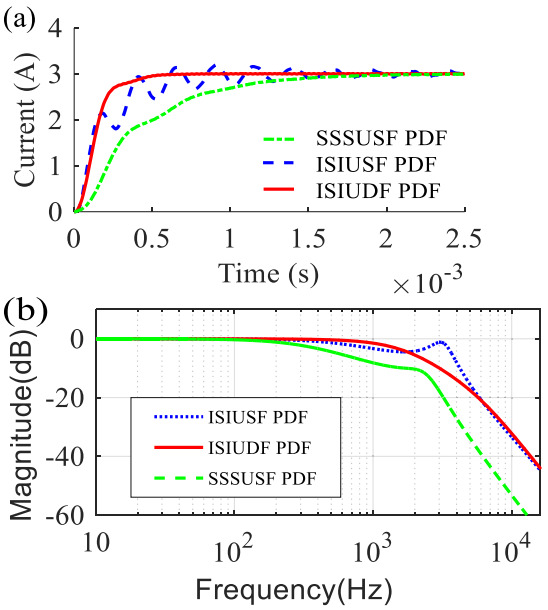

FIGURE 14. Current loop responses with different control strategies (a: Time domain, b: Frequency domain).

TABLE 4. Variable speed response system performance indicators.

Control strategy	Settling time	Overshoot
ISIUDF PDF+PI	104 ms	15.7%
ISIUDF PDF+MPM PDF	116 ms	-
ISIUDF PDF+TPM PDF	72 ms	-

A step change speed command is given in the range of 1000 rpm to 2000 rpm to verify the system's ability to track acceleration and deceleration commands. The responses of the speed loop using the three control strategies are shown in Fig. 15, and the dynamic performance characteristics of the system are presented in Table 4. The three control strategies can accurately track the speed command without static error during system acceleration and deceleration. The ISIUDF PDF+PI control has the shortest rise time among the three control strategies, but the response has an overshoot of 15.7%, which extends the settling time of the system. Both PDF control strategies can track the speed command without overshoot during the acceleration and deceleration processes. However, in terms of settling time, ISIUDF PDF+TPM PDF shows better dynamic performance than ISIUDF PDF+MPM PDF control strategy.

In the complex industrial control environment, there are mainly two factors that cause the disturbance of the motor load torque. One is the sudden load which causes the system

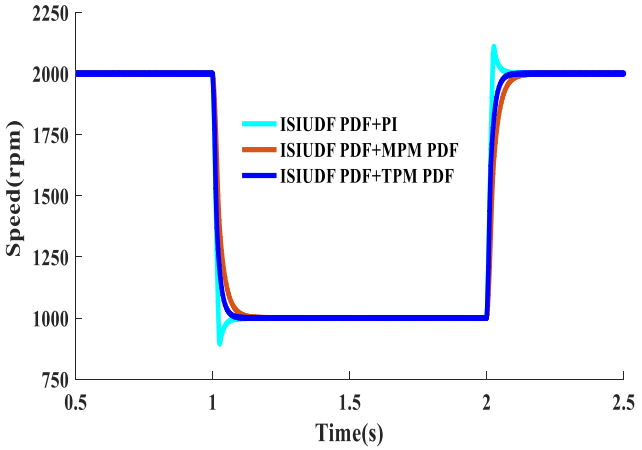

FIGURE 15. Variable speed response diagram.

TABLE 5. The Performance indicators of disturbance response system.

Control strategy	Speed fluctuation rate (Randomly variable load)	Speed fluctuation rate (Sudden load)
ISIUDF PDF+PI	2.61%	6.55%
ISIUDF PDF+MPM PDF	0.5%	2.32%
ISIUDF PDF+TPM PDF	0.3%	1.42%

*Speed fluctuation rate = maximum value of speed fluctuation /speed command amplitude

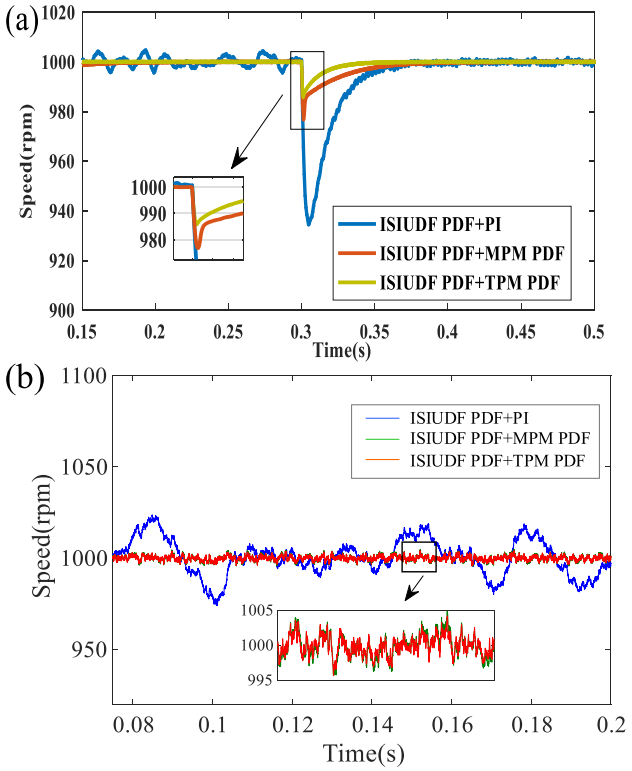

FIGURE 16. Disturbance responses (a: Sudden load, b: Randomly variable load).

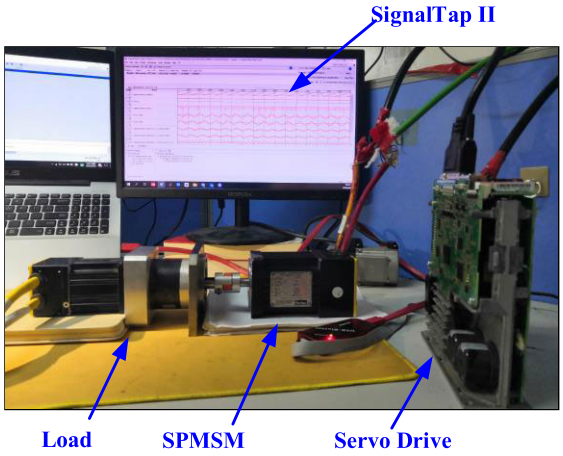

FIGURE 17. Experimental platform.

speed to fluctuate, such as gear meshing, heavy object grabbing. If the rotational speed fluctuates too much or the time to return to the speed command is too long, the control performance of the system is affected. The other factor is random disturbance which is characterized by a small scale and irregularity, such as workpiece surface processing, robot joint friction. For systems with poor disturbance rejection, random disturbance causes fluctuations in speed response and affects system control accuracy. The disturbance rejection of the speed loop with the three control strategies are compared. Given a speed command of 1000rpm, after the system speed stabilizes, a sudden load torque of 0.3Nm and a random disturbance torque of 0.01Nm are applied, respectively. The system response is shown in Fig. 16, and the disturbance performance indicators are shown in Table 5. For sudden load disturbances, Fig. 16(a) shows that the ISIUDF PDF+PI control strategy has larger speed response fluctuations and longer response time. The ISIUDF PDF+MPM PDF control strategy has a weaker ability to suppress load fluctuations than the ISIUDF PDF+TPM PDF control strategy. For random disturbances, Fig. 16(b) shows that the speed fluctuation of the ISIUDF PDF+PI control strategy is greater than the speed fluctuations of the two PDF control strategies, and the latter is more robust.

B. EXPERIMENTAL VERIFICATION

Fig. 17 is the motor control platform for this experiment, which mainly includes servo driver, load mechanism, Parker N070F series SPMSM, PC and Altera's EP4CE15 series FPGA chip. Data were captured and generated by Signal Tap II of the software Quartus II, and the load is simulated by the motor-to-drag method.

In order to further verify the effectiveness of the algorithm and PWM update strategy proposed in this paper for improving the current loop bandwidth, we have carried out the following current loop experiment. When the motor is under load conditions, the down-sampling rate of the Sinc3 filter is set, and the 35% rated current step command of the q-axis is given to maintain the motor speed at about 30% of the rated speed to reduce the impact of the drive's PWM dead time and dynamic and static friction on the torque.

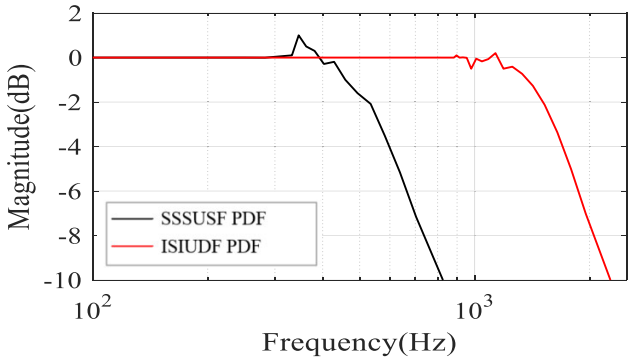

FIGURE 18. Amplitude-frequency characteristics of different PDF current loop control strategies.

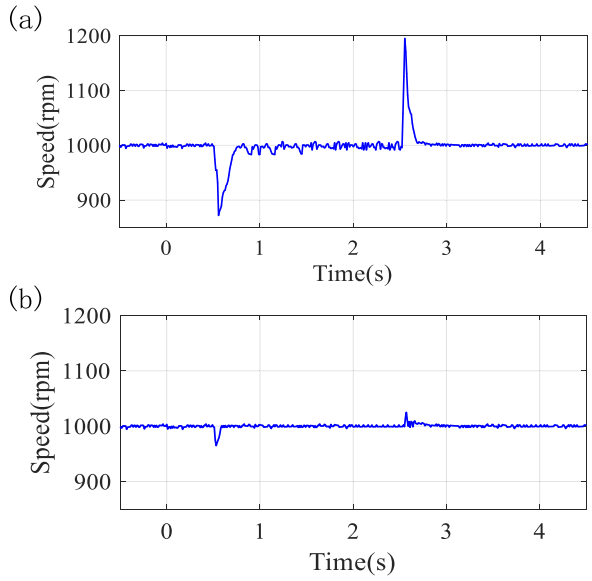

FIGURE 19. Comparison of disturbance responses (a: ISIUDF PDF+PI control strategy, b: ISIUDF PDF+TPM PDF control strategy).

Then, the q-axis is given a sinusoidal current signal with an amplitude of 10% of the motor's rated current. The signal frequency is gradually increased from 10 Hz to the maximum test frequency value, the feedback current is recorded, and the amplitude-frequency characteristic curve of the current loop under different PDF control strategies is measured. The attenuation of the feedback current signal amplitude is recorded every 50 Hz within the frequency sweep signal range. The amplitude-frequency characteristics of the current loop with the SSSUSF PDF and ISIUDF PDF control strategies are plotted in Fig. 18. With the SSSUSF PDF control strategy, the bandwidth of the current loop is about 420 Hz, and a convex peak appears at 350 Hz. However, the ISIUDF PDF control strategy reaches a bandwidth of about 940 Hz with no obvious convex peak, which indicates the proposed control strategy can significantly expand bandwidth of the current loop.

In order to verify the disturbance rejection of the improved PDF control strategy, the ISIUDF PDF control strategy is adopted in the current loop, and we have carried out the following speed loop experiment. The speed command is set to 1000 rpm, after the motor speed stabilized, a torque of 0.25 Nm is added to the motor shaft by the load mechanism and it is removed after 2 s. The speed responses under the ISIUDF PDF+PI and ISIUDF PDF+TPM PDF are recorded and compared. The system speed response is shown in Fig. 19. When the load torque changes suddenly, under the ISIUDF PDF+PI control strategy, the speed fluctuates by ±130 rpm, the fluctuation rate reaches 13%, and the speed recovery time is 220 ms. However, the speed for the ISIUDF PDF+TPM PDF control strategy only fluctuates by ±27 rpm, the fluctuation rate is only 2.7% almost as the same as ISIUDF PDF+MPM PDF control strategy, and the speed recovery time is negligible. The experimental results show that the ISIUDF PDF+TPM PDF control strategy can effectively improve the disturbance rejection of the system.

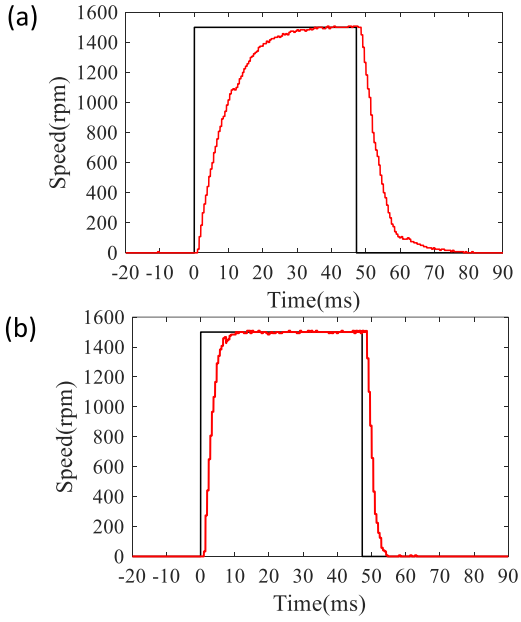

FIGURE 20. Speed responses comparison (a: ISIUDF PDF+MPM PDF control strategy, b: ISIUDF PDF+TPM PDF control strategy).

When the motor is under no-load conditions, a square wave speed command is given with an amplitude of 0–1500 rpm, and the speed feedback under different control strategies is recorded for comparison and analysis. Fig. 20 shows the system speed responses using the ISIUDF PDF+MPM PDF control strategy and the ISIUDF PDF+TPM PDF control strategy, respectively. With the ISIUDF PDF+MPM PDF control strategy, the speed response can track the speed within 30 ms, which is a substantial improvement in the dynamic response performance of the system. However, the ISIUDF PDF+TPM PDF control strategy further shortens the tracking time for the speed response to about 10 ms, and the dynamic response performance of the system is improved.

VI. CONCLUSION

In this paper, an optimal double-loop PDF control strategy was proposed for high performance servo applications

of PMSM. The influence of the location distribution of the characteristic roots on the dynamic performance of the closed-loop system was analyzed. In order to improve the system dynamics and reduce the influence of sampling delay on the system, a double-feedback PDF control strategy of ISIU was proposed. The PDF parameters tuning methods of the current loop and speed loop were derived and the corresponding hardware timing diagram was designed based on the asynchronous double-loop PDF structure of FPGA. Simulations and experimental results show that the proposed double-loop PDF control strategy can greatly expand the bandwidth of the current loop without changing the switching frequency, and significantly improve the dynamic performance and disturbance rejection of the system.

REFERENCES

[1] S. Lu and X. Wang, "Observer-based command filtered adaptive neural network tracking control for fractional-order chaotic PMSM," *IEEE Access*, vol. 7, no. 1, pp. 88777–88788, Jul. 2019.

[2] K. Liu, C. Hou, and W. Hua, "A novel inertia identification method and its application in PI controllers of PMSM drives," *IEEE Access*, vol. 7, no. 1, pp. 13445–13454, Feb. 2019.

[3] T. Yuan, D. Wang, X. Wang, X. Wang, and Z. Sun, "High-precision servo control of industrial robot driven by PMSM-DTC utilizing composite active vectors," *IEEE Access*, vol. 7, pp. 7577–7587, Jan. 2019, doi: 10.1109/ACCESS.2018.2890539.

[4] X. Chen, S. Yuan, and Z. Peng, "Nonlinear vibration for PMSM used in HEV considering mechanical and magnetic coupling effects," *Nonlinear Dyn.*, vol. 80, no. 1, pp. 541–552, Jan. 2015.

[5] G.-M. Sung, C.-P. Yu, T.-W. Hung, and H.-Y. Hsieh, "Mixed-mode chip implementation of digital space SVPWM with simplified-CPU and 12-bit 2.56 Ms/s switched-current delta-sigma ADC in motor drive," *IEEE Trans. Power Electron.*, vol. 27, no. 2, pp. 916–930, Feb. 2012.

[6] Y.-K. Cho, M.-D. Kim, and C.-Y. Kim, "A low switching noise and high-efficiency buck converter using a continuous-time reconfigurable delta-sigma modulator," *IEEE Trans. Power Electron.*, vol. 33, no. 12, pp. 10501–10511, Dec. 2018, doi: 10.1109/TPEL.2018.2806360.

[7] P. Tety, A. Konate, O. Asseu, E. Soro, P. Yoboue, and A. R. Kouadjo, "A robust extended Kalman filter for speed-sensorless control of a linearized and decoupled PMSM drive," *Engineering*, vol. 07, no. 10, pp. 691–699, Oct. 2015, doi: 10.4236/eng.2015.710060.

[8] Z. Kuang, B. Du, S. Cui, and C. C. Chan, "Speed control of load torque feedforward compensation based on linear active disturbance rejection for five-phase PMSM," *IEEE Access*, vol. 7, pp. 159787–159796, Nov. 2019, doi: 10.1109/ACCESS.2019.2950368.

[9] M. Marufuzzaman, M. B. I. Reaz, L. F. Rahman, and T. G. Chang, "A high speed current dq PI controller for PMSM drive," *Tehnički Vjesnik*, vol. 21, no. 3, pp. 467–470, Jun. 2014.

[10] L. Rovere, A. Formentini, and P. Zanchetta, "FPGA implementation of a novel oversampling deadbeat controller for PMSM drives," *IEEE Trans. Ind. Electron.*, vol. 66, no. 5, pp. 3731–3741, May 2019, doi: 10.1109/TIE.2018.2851994.

[11] M. H. Vafaie, B. M. Dehkordi, P. Moallem, and A. Kiyoumarsi, "A new predictive direct torque control method for improving both steady-state and transient-state operations of the PMSM," *IEEE Trans. Power Electron.*, vol. 31, no. 5, pp. 3738–3753, May 2016.

[12] W. H. Wang and X. Xiao, "Adaptive incremental predictive control method for current of PMSM based on online identification of inductance," *Electr. Mach. Control*, vol. 18, no. 2, pp. 75–82, Feb. 2014.

[13] M. Yang, X. Lang, J. Long, and D. Xu, "Flux immunity robust predictive current control with incremental model and extended state observer for PMSM drive," *IEEE Trans. Power Electron.*, vol. 32, no. 12, pp. 9267–9279, Dec. 2017.

[14] J. Q. Sun and Y. P. You, "PMSM speed control system based on linear active-disturbance-rejection control," *Modern Electron. Techn.*, vol. 37, no. 16, pp. 152–155, Aug. 2014.

[15] H. H. Choi, E. K. Kim, D. Y. Yu, J. W. Jung, and T. H. Kim, "Precise PI speed control of permanent magnet synchronous motor with a simple learning feedforward compensation," *Electr. Eng.*, vol. 99, no. 1, pp. 133–139, Mar. 2017.

[16] W. Guo and C. W. Zhang, "Fuzzy PI speed controller optimal design for PMSM drives," *Lect. Notes Electr. Eng.*, vol. 121, no. 5, pp. 565–571, Nov. 2011.

[17] Y. L. Gong and Y. Y. Qu, "The design of adaptive PI speed controller for permanent magnet synchronous motor servo system," *Lect. Notes Electr. Eng.*, vol. 107, no. 1, pp. 783–791, Jan. 2012.

[18] X. Wang, M. Tang, and Y. BuBai, "Robustness analysis of PDF control for elect-hydraulic servo system," in *Proc. 2nd Int. Conf. Mech. Electron. Eng.*, Kyoto, Japan, Aug. 2010, pp. V2–196, doi: 10.1109/ICMEE.2010.5558446.

[19] B. Y. Bo, T. Meng, and H. Li, "Design and simulation for electromotor speed regulation system based on PDF control strategy," *J. Chongqing Univ. Technol. Natural*, vol. 25, no. 8, pp. 52–59, Aug. 2011.

[20] S. Cheng and C.-W. Li, "Fuzzy PDFF-IIR controller for PMSM drive systems," *Control Eng. Pract.*, vol. 19, no. 8, pp. 828–835, Aug. 2011.

[21] A. Karthikeyan and C. Nagamani, "FPGA based direct torque control with speed loop pseudo derivative controller for PMSM drive," *Cluster Comput.*, vol. 22, no. 6, pp. 13511–13519, Feb. 2018.

[22] K. K. Prabhakaran, B. V. Perumal, A. Karthikeyan, and C. Nagamani, "Speed loop pseudo derivative feedback controller based direct torque controlled permanent magnet synchronous motor drive," in *Proc. IEEE 7th Power India Int. Conf. (PIICON)*, Bikaner, India, Nov. 2016, pp. 1–5, doi: 10.1109/POWERI.2016.8077247.

[23] Q. Xing, M. Tang, and B. Zhang, "Anti-disturbance pseudo-differential feedback strategy motor control based on load observation," *Inf. Control*, vol. 44, no. 2, pp. 142–146, Apr. 2015, doi: 10.13976/j.cnki.xk.2015.0142.

[24] A. Karthikeyan, K. K. Prabhakaran, B. V. Perumal, and C. Nagamani, "Pseudo derivative feedback current controlled sensorless PMSM drive with flux-torque based MRAS estimator for low speed operation," in *Proc. IEEE Int. Symp. Sensorless Control Electr. Drives (SLED)*, Catania, Italy, Sep. 2017, pp. 115–120, doi: 10.1109/SLED.2017.8078440.

[25] H. Li, Z. Nie, and F. Hu, "Stability analysis for matrix converter fed permanent magnet synchronous motor system based on PDF control," in *Proc. 17th Int. Conf. Electr. Mach. Syst. (ICEMS)*, Hangzhou, China, Oct. 2014, pp. 3313–3317, doi: 10.1109/ICEMS.2014.7014064.

[26] X. Q. Tang, L. H. Su, X. D. Zhou, and J. J. Cheng, "Bandwidth expansion of current loop for AC servo system based on FPGA," *J. Huazhong Univ. Sci. Technol., Natural Sci. Ed.*, vol. 42, no. 2, pp. 1–5, Feb. 2014.

[27] B. Jacob and M. R. Baiju, "Simple multilevel inverter-based induction motor drive scheme using sigma-delta converter with space-vector quantiser," *IET Power Electron.*, vol. 5, no. 8, pp. 1483–1490, Sep. 2012.

[28] S.-H. Song, J.-W. Choi, and S.-K. Sul, "Current measurements in digitally controlled AC drives," *IEEE Ind. Appl. Mag.*, vol. 6, no. 4, pp. 51–62, Jul./Aug. 2000.

[29] J. Bocker, S. Beineke, and A. Bahr, "On the control bandwidth of servo drives," in *Proc. 13th Eur. Conf. Power Electron. Appl.*, Barcelona, Spain, 2009, pp. 1–10.

[30] B. Li and M. Tang, "Design and performance simulation in integrated platform control system based on PDF algorithm for varied-load object," *Chin. J. Eng. Des.*, vol. 20, no. 1, pp. 49–54, Feb. 2013, doi: 10.3785/j.issn.1006-754X.2013.01.011.

HAITAO DONG was born in 1975. He received the Ph.D. degree from the School of Mechanical Science and Engineering, Huazhong University of Science and Technology, Wuhan, China, in 2012.

He currently works with the School of Mechanical Engineering, Guangxi University. His main research interests include high-performance servo drive technology, robot control, industrial Ethernet, and numerical control technology.

MINGCHEN XIAO was born in 1996. He received the B.E. degree in mechanical engineering from Hainan University, Haikou, China, in 2018, and the M.E. degree in mechanical engineering from Guangxi University, Nanning, in 2020.

His research interest includes dynamic analysis and control of PMSM.

ZHAOJUN LI was born in 1964. He received the Ph.D. degree from the School of Mechanical Science and Engineering, Huazhong University of Science and Technology, Wuhan, China, in 2006.

He currently works with the School of Mechanical Engineering, Guangxi University. His research interests include measurement technology and electromechanical system dynamics.

SHUAITAO ZHANG was born in 1997. He received the B.E. degree in mechanical engineering from Zhengzhou University, Zhengzhou, China, in 2020. He is currently pursuing the M.E. degree in mechanical engineering with Guangxi University, Nanning.

His research interests include industrial Ethernet and dynamic analysis of PMSM.

JIANGUO CHEN was born in 1997. He received the B.E. degree in mechanical engineering from Guangxi University, Nanning, China, in 2020, where he is currently pursuing the M.E. degree.

His research interests include parameter identification of PMSM and high-performance servo drive technology.